Science of the Total Environment 795 (2021) 148778

Contents lists available at ScienceDirect

Science of the Total Environment

journal homepage: www.elsevier.com/locate/scitotenv

The skeleton of *Balanophyllia* coral species suggests adaptive traits linked to the onset of mixotrophy

Quinzia Palazzo [a,g,1], Fiorella Prada [b,g,1], Tim Steffens [c], Simona Fermani [a,h], Chiara Samorì [a], Giacomo Bernardi [d], Alexis Terrón-Sigler [e,i], Francesca Sparla [f,*], Giuseppe Falini [a,g,j,**], Stefano Goffredo [b,g,**]

[a] Department of Chemistry <<Giacomo Ciamician>>, University of Bologna, Via Selmi 2, 40126 Bologna, Italy
[b] Marine Science Group, Department of Biological, Geological and Environmental Sciences, University of Bologna, Via Selmi 3, 40126 Bologna, Italy
[c] Xell AG, Waldweg 21, 33758 Schloss Holte-Stukenbrock, Germany
[d] Department of Ecology and Evolutionary Biology, University of California Santa Cruz, 115 McAllister Way, Santa Cruz, CA 95060, USA
[e] Departamento de Zoología, Facultad de Biología, Universidad de Sevilla, Avda. Reina Mercedes 6, 41012 Sevilla, Spain
[f] Department of Pharmacy and Biotechnology, University of Bologna, Via Irnerio 42, 40126 Bologna, Italy
[g] Fano Marine Center, The Inter-Institute Center for Research on Marine Biodiversity, Resources and Biotechnologies, Viale Adriatico 1/N, 61032 Fano, Italy
[h] CIRI Health Sciences & Technologies (HST), University of Bologna, I-40064 Bologna, Italy
[i] Asociacion Hombre y Territorio, C/Betania no. 13, CP. 41007 Sevilla, Spain
[j] Consiglio Nazionale delle Ricerche, Istituto per lo Studio dei Materiali Nanostrutturati (CNR-ISMN), Via P. Gobetti 101, 40129 Bologna, Italy

HIGHLIGHTS

- Preserved skeletal structural features in *Balanophyllia* azooxanthellate species.
- The onset of mixotrophy led to larger, denser and less porous coral skeletons.
- Higher amount of intra-skeletal organic matrix found in zooxanthellate species.
- Skeletal protein migration differs between azooxanthellate and zooxanthellate species.
- Crystallographic features preserved regardless of trophic strategy.

GRAPHICAL ABSTRACT

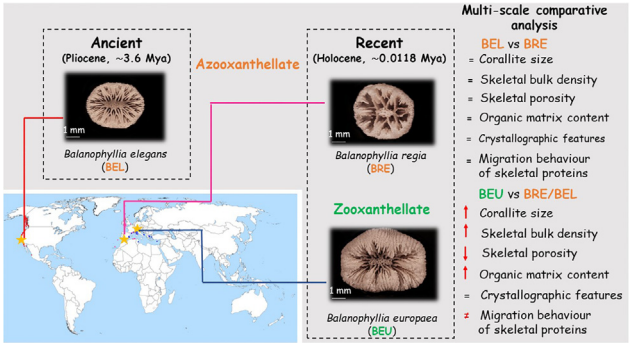

ARTICLE INFO

Article history:
Received 26 April 2021
Received in revised form 26 June 2021
Accepted 27 June 2021
Available online 1 July 2021

Editor: Henner Hollert

Keywords:
Balanophyllia
Skeletal features
Intra-skeletal organic matrix

ABSTRACT

The diversity in the skeletal features of coral species is an outcome of their evolution, distribution and habitat. Here, we explored, from macro- to nano-scale, the skeletal structural and compositional characteristics of three coral species belonging to the genus *Balanophyllia* having different trophic strategies. The goal is to address whether the onset of mixotrophy influenced the skeletal features of *B. elegans*, *B. regia*, and *B. europaea*. The macroscale data suggest that the presence of symbiotic algae in *B. europaea* can lead to a surplus of energy input that increases its growth rate and skeletal bulk density, leading to larger and denser corals compared to the azooxanthellate ones, *B. regia* and *B. elegans*. The symbiosis would also explain the higher intra-skeletal organic matrix (OM) content, which is constituted by macromolecules promoting the calcification, in *B. europaea* compared to the azooxanthellate species. The characterization of the soluble OM also revealed differences between *B. europaea* and the azooxanthellate species, which may be linked to diverse macromolecular machineries responsible for skeletal biosynthesis and final morphology. Differently, the crystallographic features were homogenous among species, suggesting that the basic building blocks of skeletons remained a conserved trait

* Corresponding author.
** Corresponding authors at: Fano Marine Center, The Inter-Institute Center for Research on Marine Biodiversity, Resources and Biotechnologies, Viale Adriatico 1/N, 61032 Fano, Italy.
E-mail addresses: francesca.sparla@unibo.it (F. Sparla), giuseppe.falini@unibo.it (G. Falini), s.goffredo@unibo.it (S. Goffredo).
[1] Equally contributing authors.

https://doi.org/10.1016/j.scitotenv.2021.148778

Biomineralization
Trophic strategy

in these related species, regardless of the trophic strategy. These results show changes in skeletal phenotype that could be triggered by the onset of mixotrophy, as a consequence of the symbiotic association, displaying remarkable plasticity of coral skeletons which repeatedly allowed this coral group to adapt to a range of changing environments throughout its geological history.

1. Introduction

Scleractinian corals are an important group of organisms responsible for creating the framework of reefs and exerting important controls on global climate and the marine environment (Dishon et al., 2020). The evolutionary history of Scleractinia has long been tackled through: 1) traditional systematics based on an analysis of the macro scale skeletal characters (Cairns, 2001) and 2) molecular phylogenetics (Arrigoni et al., 2014). The incongruence between traditional and molecular systematics has stimulated the search for new fine-scale micromorphological and microstructural characters, both in the skeleton and soft tissue (Arrigoni et al., 2014; Terrón-Sigler and López-González, 2005).

Among Scleractinia, the genus *Balanophyllia* has ~50 species and a world-wide distribution (Vaughan and Wells, 1943). The distribution of these species is the result of several factors (e.g., larval dispersal ability, environmental conditions) which had important consequences for biogeography and species evolution, which include intrinsic larval dispersal ability (Gerrodette, 1981). The genus *Balanophyllia* has colonized the Mediterranean Sea since the Miocene or at least the early Pliocene (Vertino et al., 2014). During the Late Miocene (~ 7.2 to 5.3 Mya) the Mediterranean Sea underwent one of its most dramatic changes causing the extinction of many species and the shallow-water coral-reef province (Vertino et al., 2014). The causes that led to the regression of the Mediterranean coral fauna diversity are supposed to be: 1) the Messinian Salinity Crisis, 2) the closure of the open marine seaway through the Middle East (Bosellini and Perrin, 2008), and 3) the decreasing seawater surface temperature (Martín et al., 2012). Therefore, the environmental conditions of the Mediterranean varied enormously during the late Miocene, and these modifications may have acted as driving forces for the acquisition of the symbiosis in the *Balanophyllia* genus, resulting in an evolutionary advantage in the highly oligotrophic Mediterranean Sea (Stanley, 2003) which led to the appearance of *Balanophyllia europaea* in the Pleistocene (~2.5–0.0117 Mya) (Vertino et al., 2014).

Subtle differences in growth form, algal symbiosis, sexual system and life history traits confer advantages to growth under certain environmental conditions among species of the same genus (Pandolfi and Jackson, 2001) and these differences are generally established over millions of years. The genus *Balanophyllia* offers a unique opportunity to perform a comparative study among phylogenetically related species characterized by different energy intake strategies, namely zooxanthellate and azooxanthellate species. In particular, the current study was performed on two azooxanthellate corals, namely *B. elegans and B. regia,* and the zooxanthellate *B. europaea*. The first appearance in the fossil record of the species *B. elegans* dates back to the middle Pliocene (~ 5.3 to 2.6 Mya) on the Pacific Coast of North America (Gerrodette, 1981). The Pacific Ocean during the Paleogene (between 65 and 23 Ma) was connected to the other oceans (Lyle et al., 2008) until the closure of the Panama Gateway around 3 Ma (Coates and Obando, 1996). *B. elegans* has been detected only in the Eastern Pacific, from Alaska, USA, to Baja California, Mexico. To the best of our knowledge, no *Balanophyllia* species has been found to inhabit simultaneously the American Pacific and Atlantic coast and no amphi-Atlantic species have been reported so far. The lack of ecological and genetic information of this genus makes difficult the reconstruction of an exhaustive framework of the evolution and genetic connectivity.

Balanophyllia europaea's recent history compared to *B. elegans* and *B. regia* is supported by the fact that the former is zooxanthellate and that it is the only species in the genus *Balanophyllia* that exhibits hermaphroditism (Goffredo et al., 2000; Goffredo et al., 2004). In fact, strong evidence suggests that once the symbiosis is acquired, reverting to an azooxanthellate mode is highly unlikely, if not impossible (Campoy et al., 2020). The symbiosis provides zooxanthellate corals with additional energy compared to the azooxanthellate species, which is reflected in fast metabolism and generally higher calcification rates in the former (Stanley and van de Schootbrugge, 2009). Thus, losing the symbiotic association and adapting to an entirely heterotrophic feeding strategy would be disadvantageous in evolutionary terms. In light of the above considerations, it is reasonable to hypothesize that the zooxanthellate *B. europaea,* evolved from the azooxanthellate *B. regia*, which survived the Messinian salinity crisis in the Late Miocene. Another supporting evidence that *B. europaea* is the most recent species among those investigated in this study, is related to the mating system. In fact, studies have shown that gonochorism is over 100 times more likely to be lost than gained, since it may represent an adaptation to a sessile lifestyle by increasing the probability of finding each sex in a given area (Kerr et al., 2011). Therefore, the sexual modes might have been a trait under selection during the Mediterranean Late Miocene scenario, showing a switch from gonochorism to hermaphrodism, as a consequence of environmental change.

B. elegans (Verrill, 1864) is an aragonitic scleractinian solitary azooxanthellate coral typically found in the subtidal down to ~300 m in depth. *B. elegans* reproduces only sexually, is gonochoric, and broods its embryos (Fadlallah and Pearse, 1982). It generally occurs on the top, middle, and near the base of vertical surfaces of rocks (Foster et al., 2013). Its average linear extension rates are 0.64 ± 0.56 mm yr^{-1} (average $\pm$ SD), measured off the coast of Southern California (USA), where abundance at 7–13 m depth averaged more than 500 individuals per m^2 (Fadlallah, 1983a). Growth in *B. elegans* slows asymptotically with increase in size.

B. regia (Gosse, 1860) is an aragonitic scleractinian solitary azooxanthellate coral, rarely fused forming pseudocolonies (Zibrowius, 1980). The reproductive mode is brooding while the sexual condition is assumed to be gonochoric since *Balanophyllia europaea* is considered the only hermaphrodite species of the genus (Goffredo et al., 2000; Fadlallah, 1983b). However, further studies are needed to verify this assumption. It lives on rocky shores from very shallow water down to 25 m depth and occurs in the Mediterranean Sea and northeastern Atlantic from southeast Ireland and England to Morocco and the Canary Islands (Zibrowius, 1980). Its average linear extension rate, measured off the coast of South Finistère (Northern France), is 1.09 ± 0.47 mm yr^{-1} and decreases with size/age (Brahmi et al., 2010).

B. europaea (Risso, 1826) is an aragonitic scleractinian solitary coral and it is the only zooxanthellate species of the genus *Balanophyllia*. Because of its symbiosis with zooxanthellae it colonizes rocky shores exposed to light from near the surface to 50 m depth (Zibrowius, 1980), with abundances of more than 100 individuals m^2 (Goffredo et al., 2004). In the well-characterized populations of the northwestern Mediterranean Sea, the oral disc of *B. europaea* becomes more oval as it grows older (Goffredo et al., 2007) skeletal growth decreases with age (Goffredo et al., 2008). Its average linear extension rate, measured in the Genoa population (Northern Italy), where it was collected for the current study, is 1.17 ± 0.04 mm yr^{-1} (Goffredo et al., 2009).

B. europaea is endemic to the Mediterranean Sea and is a hermaphroditic brooding species.

Coral species descriptions were traditionally based solely on skeletal morphology. However, coral skeletal features are known to exhibit variations unrelated to evolutionary divergence and linked to other factors (e.g., different environments and ecological niches), which may explain why coral species are notoriously difficult to identify, hindering our ability to understand their ecology, evolution, and biodiversity (Todd, 2008). This multi-scale comparative analysis of the skeletal structural and compositional features of three related coral species belonging to the genus *Balanophyllia* and characterized by different trophic strategies aimed to assess whether the investigated skeletal features were more influenced by the onset of mixotrophy.

2. Materials and methods

Coral skeletal features were investigated using experimental techniques that allow multi-scale analysis (Fig. S1).

2.1. Coral collection and treatment

B. elegans specimens ($n = 65$) were randomly collected by SCUBA diving on May 10th 2017 at ~25 m depth off the California coast at Pacific Grove (36° 37′ 18″ N 121° 53′ 53″ W; Fig. S2). The samples were retrieved on exposed large rocks fixed to the sea bottom (not small boulders), where also the cup coral *Astrangia* is also present. *B. regia* specimens ($n = 67$) were randomly collected on February 7th 2017 at 8 m depth along the Granada coast, southern Iberian Peninsula, on Marina del Este beach, specifically in the Punta de la Mona (36° 43′ 08″ N 3° 43′ 38″ W; Fig. S2), where hydrodynamism is generally low (Terrón-Sigler et al., 2016). *B. europaea* specimens ($n = 116$) were randomly collected was collected on March 11th 2017 at 8–9 m depth in a rocky shore site (Punta Chiappa), east of Genoa, Italy (44° 21′ 44.54" N, 9° 07′ 49.17″ E; Ligurian Sea, North-Western Mediterranean Sea; Fig. S2), near the Marine Protected Area of Portofino, characterized by strong hydrodynamism (Misic et al., 2011). Details on coral treatments and preparation of the coral skeleton for destructive analysis are provided in the additional methods section of Appendix A Supplementary data.

2.2. Biometric parameters

Skeletal length (L: maximum axis of the oral disc), width (W: minor axis of the oral disc) and height (h: oral-aboral axis) were measured using a caliper (Goffredo et al., 2007). For each species, samples were divided in three length classes (small, medium, large) by dividing the maximum length value by three. This allowed us to account for possible differences related to the life stage of the corals, as previous studies conducted on one of the three investigated, as well as in other scleractinian corals, have shown a strong relationship between length and age. species (Goffredo et al., 2004; Goffredo et al., 2008). Dry corallite mass (M) was determined with an Ohaus Explorer Pro analytical balance (±0.0001 g) (Caroselli et al., 2011). Surface/volume (S/V) ratio was obtained by dividing S by V, where V is the total volume of the skeleton including its opened pores (obtained by buoyant weight), and S is the surface of the coral, obtained as a sum of the surface of the oral disc $\pi \times (L/2) \times (W/2)$ and the lateral surface of the coral obtained with the formula $\pi \times [3 \times (\frac{L}{2} + \frac{W}{2}) - \sqrt{(3 \times \frac{L}{2} + \frac{W}{2}) \times (L/2 + 3 \times W/2)}] \times h$ (Caroselli et al., 2015), excluding the base in contact with the substratum.

2.3. Skeletal parameters

Skeletal parameters (i.e., micro-density, bulk density and porosity) were obtained by buoyant weight using a hydrostatic balance (±0.0001 g, Ohaus Corp., Pine Brook, NJ, USA) following a standard non-destructive protocol (Caroselli et al., 2011). A subsample of specimens of each species were randomly selected and used for the destructive analyses.

2.4. Scanning electron microscopy (SEM) observations

One entire skeleton for each species was blued on a stub with carbon tape. The skeleton was then gold sputter (about 20 nm thick). The observations were performed using a Leica Cambridge Stereoscan 360 scanning electron microscope equipped with an Everhart&Thornley SE detector. The images were collected using a tension of 20 kV.

2.5. X-ray and high resolution X-ray powder diffraction (XRD and HR-XRD) analyses

X-ray powder diffraction (XRD) analyses were performed on 19 powdered samples of *B. europaea*, 20 of *B. regia* and 20 of *B. elegans*. High resolution X-ray powder diffraction (HR-XRD) analyses were performed on 3 powdered samples of each species. The diffractograms were collected using a PANanalytical X'Pert Pro equipped with X'Celerator detector diffractometer for a qualitative and quantitative analysis of calcium carbonate polymorphism. A quantitative analysis of the crystalline phases was performed using the software "Quanto" which is based on the Rietveld method (Marchegiani et al., 2009). Details on the XRD and HR-XRD procedures are provided in Appendix A Supplementary data. The structural parameters were refined by Rietveld analysis using the software Quanto and a Pseudo-Voigt peak shape function by CMPR software (Toby, 2005). The estimation of the crystallite size and microstrain fluctuations of aragonite crystals of the skeletons were performed using line profile analysis of the two most intense peaks of aragonite, (111) and (021), from the calculus of FWHM after a multipeak PseudoVoigt peak shape function fitting. The crystallite size for each reflection was calculated using Scherrer equation (Langford and Wilson, 1978) and the microstrain fluctuation on the diffraction peak broadening was derived by line profile analysis (Zolotoyabko, 2014).

2.6. Spectroscopic measurements

Fourier transform infrared spectroscopic (FTIR) analyses were conducted on a subset of random samples previously used for the diffractometric analysis, by using a Nicolet FTIR 380 spectrometer working in the range of wavenumbers 4000–400 cm^{-1} at a resolution of 2 cm^{-1}. Obtained qualitative data were analysed with the software EZ OMNIC (Thermo Electron Corporation). This technique was used to confirm the X-ray powder diffraction data. Details on the FTIR procedure is provided in Appendix A Supplementary data.

2.7. Thermogravimetric analysis (TGA)

Thermogravimetric analysis (TGA) was performed to estimate the Organic Matrix (OM) content, as weight percentage, of the powdered skeletons, using an SDT Q600 simultaneous thermal analysis instrument (TA instrument). From each powdered sample previously investigated through XRD, 5 to 10 mg of powder has been heated under a linear gradient from ambient (30 °C) up to 600 °C. The analyses were performed in N_2 flow from 30° to 120 °C with a heating rate of 10 °C/min, an isothermal at 120 °C for 5 min to remove the non-structural water absorbed moister, and another cycle from 120 to 600 °C with a heating rate of 10 °C/min to evaluate the structural water and the organic matrix from the weight lost between 150 °C and 450 °C.

2.8. Extraction of the intra-skeletal organic components

For each species, 2.5 g of a mix of the powdered skeletons previously investigated, has been used for the extraction of the organic components. Each powdered skeleton mixture was dispersed in 5 ml of milli-Q water and poured into a 20 cm-long osmotic tube for dialysis (MWCO = 3.5

kDa; CelluSep®, MFPI). The sealed tube was put into 1 L of 0.1 M CH_3COOH solution under stirring in order to dissolve the skeletal parts. The decalcification proceeded for 72 h. At the end, the tube containing the dissolved organic matrix (OM) was dialysed against milli-Q water until the final pH was about 6. The obtained aqueous solution containing the OM was centrifuged at 6000 rpm for 3 min to separate the soluble (SOM) and the insoluble (IOM) organic matrix fractions. These analyses were carried out as previously reported (Reggi et al., 2014).

2.9. OM lipid content and fatty acid analysis

The fatty acid (FA) components of the lipOM were analysed by gas chromatography–mass spectrometry (GC–MS) according to reported procedures (Samorì et al., 2017). The analyses were performed on at least 2 replicates of each skeleton on a number of 5 samples of *B. europaea*, 5 of *B. regia* and 4 of *B. elegans*. Details on the procedure are extensively reported in Appendix A Supplementary data.

2.10. OM amino acid composition analysis

Amino acid analysis was conducted by Ultra High Performance Liquid Chromatography (UHPLC Agilent Technologies) equipped with a diode array detector (Agilent Technologies). Macromolecules were hydrolyzed using 6 m HCl for 24 h at 100 °C. During hydrolysis, complete or partial destruction of several amino acids occurs: tryptophan is destroyed, and serine and threonine are partially destroyed. Sulphur amino acids are altered. Then samples were dried and used for derivatization with 6-Aminoquinolyl-N-hydroxysuccinimidyl carbamate (AQC). Detection occurred at a wavelength of 260 nm.

2.11. Characterization of the organic matrix

Five ml of the volume of the soluble part of the organic matrix (SOM) was previously lyophilized, weighed and then analysed using Fourier Transform InfraRed (FTIR) spectroscopy.

The remaining part of the SOM volume was used to separate the proteins by polyacrylamide gel electrophoresis (SDS-PAGE). An extensive description of the procedure is provided in Appendix A Supplementary data.

2.12. Statistical analyses

Data were checked for normality using a Kolmogorov-Smirnov test ($N > 50$) and Shapiro-Wilk test ($N < 50$) and for homogeneity using Levene's Test. One-way analysis of variance (ANOVA) and the non-parametric Kruskal–Wallis equality-of-populations rank were used to assess differences in biometric parameters, skeletal parameters, intra-skeletal organic matrix and water content, and skeletal mineralogy among size classes for each species. ANOVA was used to compare porosity, bulk density and the % composition of the main fatty acids among species. When assumptions for parametric statistics were not fulfilled, the non-parametric Kruskal–Wallis test was used, in particular for micro-density, length, width, height, surface, skeletal mass, volume, *S/V* ratio, intra-skeletal organic matrix and water content, mineral phase content and the relative zone absorption intensities of SOMs. Where significant, pairwise comparisons between species were performed via Tukey's HSD or Mann Whitney post hoc tests. To obtain information about the proportion of the skeletal growth (allometric or isometric growth), a linear regression was performed to test the relation between individual width-length and height-length for each species. We assumed that when the confidence interval (CI) of the exponent of the non-linear regression did not contain 1 it indicates an allometric growth (with a biometric parameter increasing more rapidly than another) while, when the exponent of the nonlinear regression contains 1 it indicates an isometric growth. The significance of the correlation was verified using Pearson's correlation coefficient. The statistical differences in regression slopes between the three species were examined comparing the confidence intervals of regression coefficients. All analyses were computed using SPSS Statistics 20. Finally, principal component analysis (PCA) was used to explore coral biometric parameters (length, width,

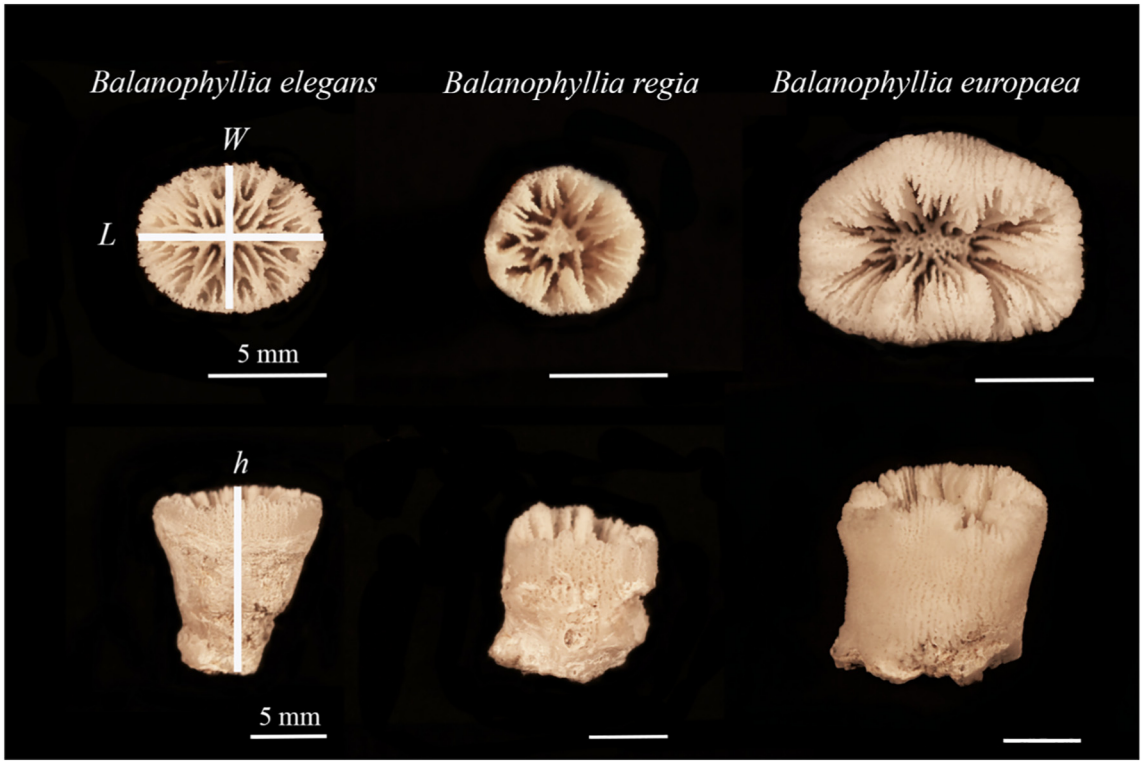

Fig. 1. *Balanophyllia elegans*, *B. regia*, *B. europaea* corallites. Lines indicate polyp length (*L*: maximum axis of the oral disc), polyp width (*W*: minimum axis of the oral disc), and polyp height (*h*: oral-aboral axis). Scale bar is set to 5 mm.

height), skeletal mass, volume, surface/volume ratio, skeletal parameters (micro-density, porosity, bulk density), structural variables (content of intraskeletal water, the organic matrix and the total weight loss), and the skeletal mineralogy (percentage of each mineral phases found in the skeletons), that drive the difference among the three species using PAST 3 software.

3. Results

Combined results of biometry, buoyant weight, SEM, XRD, FTIR, TGA, GC–MS, HPLC, SDS-PAGE revealed the detailed, multi-scale structural organization of the skeletons of three coral species of the genus *Balanophyllia*. For each species, all investigated parameters were compared among size classes and resulted homogeneous, thus the different sets of data were pooled together for comparison among the three species.

3.1. Biometric parameters

Polyp length, height, width, skeletal mass, and volume were significantly different among the three species (Kruskal–Wallis: $p < 0.001$; Fig. 1, Table 1, Fig. S3) and higher in *B. europaea* compared to *B. elegans* and *B. regia* (Mann–Whitney U: $p < 0.001$; Fig. 1, Table 1, Fig. S3). Length and height of *B. elegans* were significantly higher compared to *B. regia* (Mann–Whitney U: length $p < 0.05$; height $p < 0.01$). The surface/volume ratio (S/V) was significantly higher in both azooxanthellate corals compared to *B. europaea* (Mann–Whitney U: $p < 0.001$), while no difference was found between *B. regia* and *B. elegans* (Mann–Whitney U: $p > 0.05$; Table 1, Fig. S3). In all species, the increase of polyp width with respect to polyp length exhibited an allometric growth, with length increasing more rapidly than did width, which resulted in an oval oral disc as polyp size increased. The confidence interval CI of the regression equation exponent was <1 for all species: 0.603–0.757, 95% CI in *B. europaea*; 0.681–0.868, 95% CI in *B. regia*; 0.645–0.837, 95% CI in *B. elegans* (Table S1). The confidence interval of the exponent of the non-linear regression between polyp length and height contained 1 for both the azooxanthellate species (0.768–1.409, 95% CI in *B. regia*; 0.803–1.392, 95% CI in *B. elegans;* Table S1), indicating that coral polyp height and length have isometric growth. For the zooxanthellate *B. europaea*, the confidence interval of the exponent was >1, showing an allometric growth, with polyp height increasing more quickly than polyp length (Table S1).

3.2. Skeletal parameters

Mean skeletal parameters were significantly different among the three species (ANOVA, bulk density and porosity: $p < 0.001$; Kruskal-Wallis, micro-density: $p < 0.001$; Fig. S4). The mean micro-density was homogeneous between *B. europaea* and *B. elegans* and higher compared to *B. regia* (Mann Whitney *U* test, $p > 0.05$ and $p < 0.001$, respectively; Table 1, Fig. S4). The mean bulk density was homogeneous between *B. regia* and *B. elegans* and lower compared to *B. europaea* (Tukey's HSD post-hoc test, $p > 0.05$ and $p < 0.001$, respectively; Table 1, Fig. S4). The mean porosity was homogeneous between *B. regia* and *B. elegans* and higher compared to *B. europaea* (Tukey's HSD post-hoc test, $p > 0.05$ and $p < 0.001$, respectively; Table 1, Fig. S4).

3.3. Mineral skeletal texture

Fig. 2 reports SEM images of the coral skeletons and of mechanically fractured septa at increasing magnifications. The images of the entire skeleton clearly show the different septa organization in the three coral species. The images of cross sections of a septum were acquired for each species. These show the presence of fibrous structures and calcification centers, as previously defined in coral skeleton (Tambutté et al., 2011). The distribution of the calcification centers, as well as the size of the fibers, are difficult to quantify. A qualitative view does not show important differences in the mineralogical texture of the three species.

Table 1
Biometric parameters, skeletal parameters (micro-density, bulk density, and porosity), mineral phases and intra-skeletal organic matrix, water content, and fatty acid concentration. Data are presented as mean ± Standard Deviation (SD). Pairwise comparisons between species were performed with Mann-Whitney *U* test. Significant *p*-values are in bold. BEL = *B. elegans*, BRE = *B. regia*, BEU = *B. europaea*. * $p < 0.05$, ** $p < 0.01$, *** $p < 0.001$.

	Species			Pairwise comparison	
	BEL	BRE	BEU	Species	*p*-value
	mean (SD)	mean (SD)	mean (SD)	compared	
Length	8.61 ± 1.33	8.14 ± 1.30	12.37 ± 2.80	BEU BRE	***
(mm)	N = 65	N = 67	N = 116	BEU BEL	***
				BRE BEL	*
Width	7.07 ± 0.91	7.14 ± 0.99	9.59 ± 1.71	BEU BRE	***
(mm)	N = 65	N = 67	N = 116	BEU BEL	***
				BRE BEL	NS
Height	8.46 ± 1.96	7.69 ± 2.15	11.3 ± 3.70	BEU BRE	***
(mm)	N = 65	N = 67	N = 116	BEU BEL	***
				BRE BEL	**
Skeletal mass	0.29 ± 0.15	0.27 ± 0.18	1.25 ± 0.93	BEU BRE	***
(g)	N = 65	N = 67	N = 116	BEU BEL	***
				BRE BEL	NS
Volume	200 ± 101	194 ± 123	723 ± 537	BEU BRE	***
(mm^3)	N = 65	N = 67	N = 116	BEU BEL	***
				BRE BEL	NS
S/V ratio	1.41 ± 0.27	1.39 ± 0.37	0.82 ± 0.21	BEU BRE	***
(mm^{-1})	N = 65	N = 67	N = 116	BEU BEL	***
				BRE BEL	NS
Micro-density	2.72 ± 0.04	2.64 ± 0.07	2.71 ± 0.05	BEU BRE	***
(g/cm^3)	N = 65	N = 67	N = 116	BEU BEL	NS
				BRE BEL	***
Bulk density	1.48 ± 0.17	1.41 ± 0.18	1.72 ± 0.14	BEU BRE	***
(g/cm^3)	N = 65	N = 67	N = 116	BEU BEL	***
				BRE BEL	NS
Porosity	45.8 ± 6.26	46.3 ± 7.03	36.3 ± 5.47	BEU BRE	***
(%)	N = 65	N = 67	N = 116	BEU BEL	***
				BRE BEL	NS
Aragonite	97 ± 2.40	93 ± 4.65	98 ± 1.37	BEU BRE	**
(%)	N = 20	N = 20	*N* = 19	BEU BEL	NS
				BRE BEL	**
Magnesium-calcite	1.33 ± 1.17	3.77 ± 4.92	2.22 ± 1.28	BEU BRE	NS
(%)	N = 20	*N* = 20	N = 19	BEU BEL	*
				BRE BEL	**
Calcite	0.55 ± 0.95	2.31 ± 1.98	0.12 ± 0.38	BEU BRE	***
(%)	N = 20	N = 20	N = 19	BEU BEL	NS
				BRE BEL	**
Quartz	1.08 ± 1.48	0.9 ± 0.99	0	BEU BRE	***
(%)	N = 20	N = 20	N = 19	BEU BEL	**
				BRE BEL	NS
Water	0.67 ± 0.08	0.78 ± 0.11	0.81 ± 0.34	BEU BRE	NS
(wt%)	N = 20	N = 20	N = 19	BEU BEL	NS
				BRE BEL	**
OM	1.99 ± 0.27	2.04 ± 0.37	2.30 ± 0.44	BEU BRE	*
(wt%)	N = 20	N = 20	N = 19	BEU BEL	*
				BRE BEL	NS
Total weight loss	2.66 ± 0.32	2.82 ± 0.43	3.12 ± 0.76	BEU BRE	NS
(wt%)	N = 20	N = 20	N = 19	BEU BEL	*
				BRE BEL	NS
Fatty acid content	0.29 ± 0.05	0.17 ± 0.12	0.12 ± 0.06	BEU BRE	
(wt%)	*N* = 4	*N* = 5	N = 5	BEU BEL	NS
				BRE BEL	

3.4. Skeletal mineralogy

Other calcium carbonate mineral phases (calcite and magnesium calcite) were found in addition to aragonite in all species (Fig. 3; Figs. S5 and S6). Calcite was found in addition to aragonite in 10% of the skeletons of *B. europaea*, 80% of the skeleton of *B. regia* and 38% of

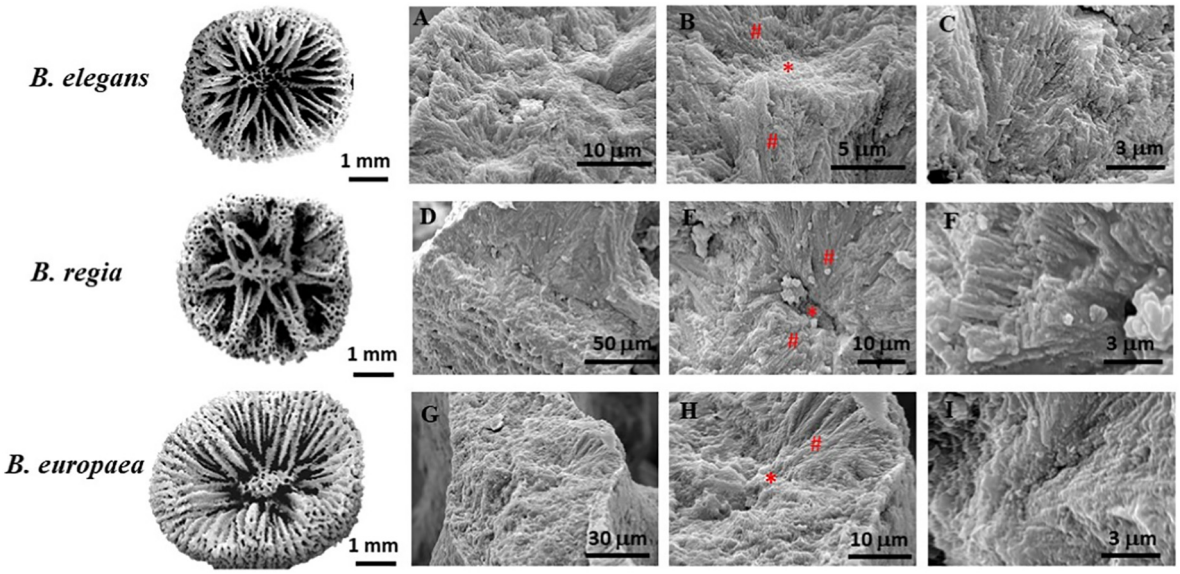

Fig. 2. Scanning electron microscopy images from coral skeleton samples of *B. elegans*, *B. regia*, and *B. europaea*. In (A-C) images at increasing magnifications of a cross section of a septum of *B. elegans* are shown. In (D—F) images at increasing magnifications of a cross section of a septum of *B. regia* are shown. In (G-I) images at increasing magnifications of a cross section of a septum of *B. europaea* are shown. * indicates the center of calcification. # indicates the fibrous region.

the *B. elegans* samples. In the remaining samples calcite content was not detectable by X-ray diffraction. Magnesium calcite was found in all the samples of the three species. In *B. regia* and *B. elegans* quartz was also detected and it was found in 70% of *B. regia* skeletons and in 48% *B. elegans* skeletons. The content in skeletal mineral phases was significantly different among the three species (Kruskal-Wallis, aragonite, calcite, quartz: $p < 0.001$, magnesium calcite, $p < 0.01$; Table 1, Fig. S5). The mean aragonite content was significantly lower in *B. regia* compared to *B. europaea* and *B. elegans* and homogeneous between *B. europaea* and *B. elegans* (Mann Whitney *U* test, $p < 0.001$ and $p > 0.05$, respectively; Table 1, Fig. 3). The content of the magnesium calcite was significantly higher in *B. regia* and in *B. europaea* compared to *B. elegans* (Mann Whitney U test, $p < 0.01$ and $p < 0.05$, respectively; Table 1, Fig. S5) and homogeneous between *B. europaea* and *B. regia* (Mann Whitney U test, $p > 0.05$; Table 1, Fig. S5). The mean calcite content was significantly higher in *B. regia* compared to *B. elegans* and *B. europaea* (Mann Whitney U test,

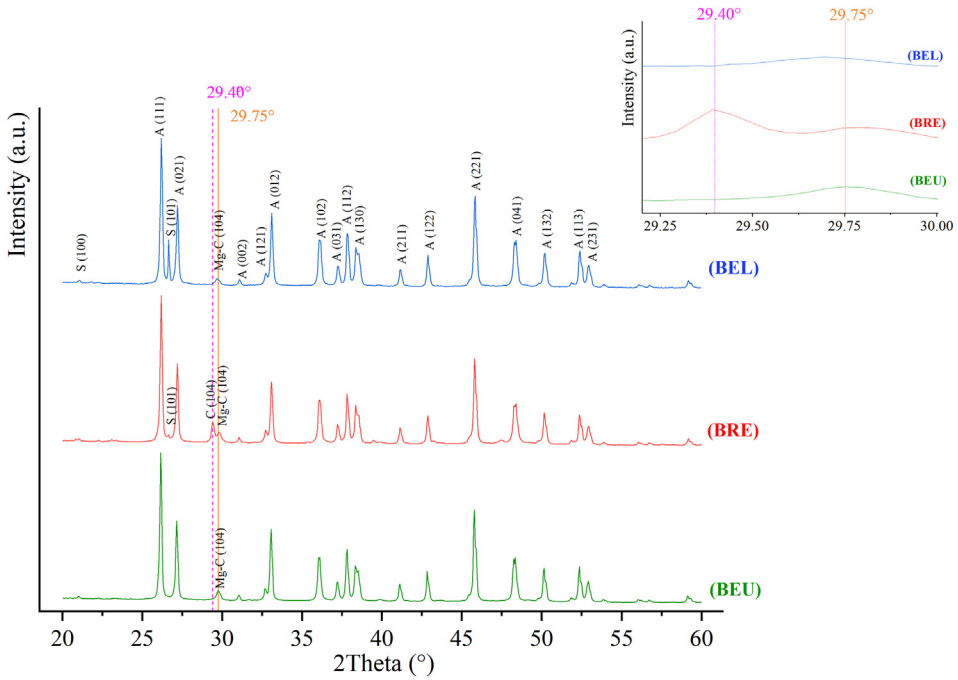

Fig. 3. X-ray powder diffraction patterns from coral skeleton samples of *B. elegans* (BEL), *B. regia* (BRE), and *B. europaea* (BEU). The characteristic diffraction peaks from aragonite (A) are observable together with weak ones from calcite (C) at 29.4°, magnesium calcite (Mg—C) at 29.75° and an additional one due to silica (S (101)) in BEL and BRE. The inserted graph is a zoom of 27.5°-32.0° diffractograms region for BEU and BRE. Notice that the max calcite peak (at 29.4°) is slightly shifted at higher 2Theta (29.75°) in corresponding of magnesium calcite. This peak asymmetry is ascribable to the isomorphic substitution of magnesium ions to calcium ions, which leads to a reduction in the calcite lattice constants thus resulting in a shift in diffraction peaks to higher 2Theta angles. The main diffraction peaks of the Miller index are indicated according to the following reference patterns: aragonite PDF 01–075–2230; calcite PDF 01–086-2336; magnesium calcium carbonate PDF 01-086-336; quartz PDF 01-085-0795.

$p < 0.01$, respectively; Table 1, Fig. 3) while no difference was found between the latter two (Mann Whitney U test, $p < 0.05$; Table 1, Fig. S5). The content of quartz did not show significant differences between the two azooxanthellate species (Mann Whitney U test, $p < 0.05$; Table 1, Fig. S5). Quartz was not found in *B. europaea*. High-resolution X-ray powder diffraction results for the planes (111) and (021) showed no variation in both crystallite size (ANOVA, $p > 0.05$) and micro-strain fluctuation (ANOVA, $p > 0.05$) among species (Tables S3 and S4).

3.5. Intra-skeletal organic matrix content

The mean intra-skeletal organic matrix (OM) and water content (% water, % OM and total weight % loss) measured by thermogravimetric analysis (TGA) were significantly different among the three species (Kruskal-Wallis: $p < 0.05$; Table 1; Figs. S7 and S8). The intra-skeletal OM content (% mass loss) was significantly higher in *B. europaea* compared to *B. regia* and *B. elegans* (Mann Whitney U test, $p < 0.05$, respectively; Table 1), while no difference was detected between the two azooxanthellate species (Mann Whitney U test, $p > 0.05$; Table 1). The intra-skeletal OM content (% mass loss) represented 1.99 ± 0.27% (mean ± SD), 2.04 ± 0.37%, and 2.30 ± 0.44% of the total weight in *B. elegans*, *B. regia*, and *B. europaea*, respectively. The intra-skeletal water content was significantly higher in *B. regia* compared to *B. elegans* (Mann Whitney U test, $p < 0.001$; Table 1), while no differences were found between *B. europaea* and the latter two (Mann Whitney U test, $p > 0.05$; Table 1). The total weight % loss (water + OM; see (Cuif et al., 2004)) was significantly higher in *B. europaea* compared to *B. elegans* (Mann Whitney U test, $p < 0.05$; Table 1), while no differences were detected compared to *B. regia* and between *B. regia* and *B. elegans* (Mann Whitney U test, $p > 0.05$, respectively; Table 1). Correlation analysis between intra-skeletal organic matrix components (water, OM and total weight % loss) and polyp length and skeletal mass revealed that the OM components do not vary with polyp length and skeletal mass in any of the species (Pearson's correlation $p > 0.05$; Table S4).

3.6. Characterization of Soluble Organic Matrix (SOM)

The chemical-physical characterization of the Soluble Organic Matrix (SOM) fractions was performed by FTIR spectroscopy and SDS-PAGE. Table S5 summarizes the observation from the FTIR spectra of SOM obtained from two extraction processes for each species (the average of the absorption peaks from two organic matrix extractions for each species are reported). In Fig. 4 the most representative spectra are shown. In general, SOM showed the same absorption bands, regardless of the coral species; however, differences were observed in their relative intensities (Table S5). In all the fractions, a weaker absorption was observed at 1734/36 cm^{-1} and a marked band at about 2924/25 cm^{-1} (which are consistent with ν C—H stretching vibration) and 28,535/4 cm^{-1}, which can be indicative of fatty acids or molecules bearing alkyl chain regions, due to the methylene and methyl groups' vibration modes. The bands at 2924 cm^{-1} and 2854 cm^{-1} were stronger in *B. regia* than *B. europaea* and *B. elegans*. Characteristic absorption bands corresponding to the protein backbone bonds were shown at 1644/55 cm^{-1} (amide I, νC=O; α-helix, random coil), at 1639 cm^{-1} (amide I; β-sheet) and at 1541/1544 cm^{-1} (amide II, νC-N). In detail, the band around 1637 cm^{-1} were observed only in the SOM from *B. europaea*, suggesting that the types of secondary structure of polypeptides are β-sheet; whereas, in the *B. regia* and *B. elegans* spectra, the band corresponding to secondary protein structure were shown only around 1644/55 cm^{-1}, which usually related to the presence of α-helix. In each SOMs the amide I was strong with respect to the amide II band. The absorption bands located in the range of 1100–950 cm^{-1} were due to glycosidic bond vibration and C—C single bond vibration modes, mainly associable to polysaccharidic moieties.

Three zones (1–3) were defined in order to estimate the relative amounts of the main functional groups of the SOMs from the FTIR spectra

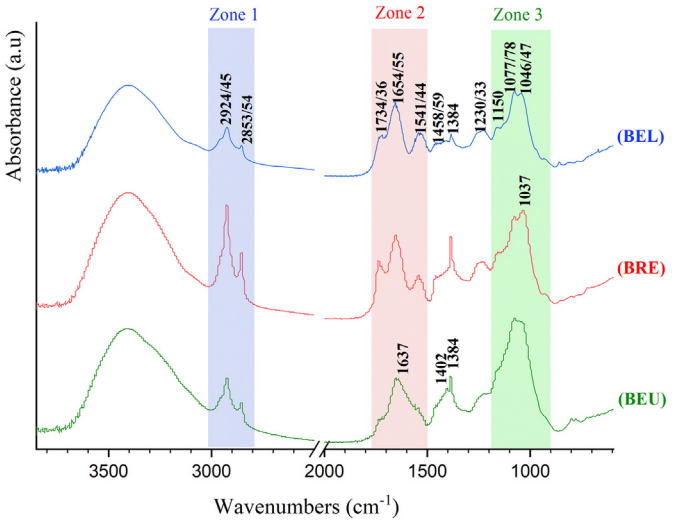

Fig. 4. FTIR spectra of intra-skeletal soluble organic matrix (SOM) extracted from the skeletons of *B. elegans* (BEL), *B. regia* (BRE), and *B. europaea* (BEU). The maximum of the absorption bands are indicated with the possible ranges of shift of absorption toward lower or upper wavenumbers. The three zones define diagnostic regions of functional groups which could be mainly associated to the presence of lipids (zone 1: 3000–2800 cm^{-1}), protein and polysaccharides (zone 2: 1750–1500 cm^{-1}) and polysaccharides (zone 3: 1100–950 cm^{-1}).

(Fig. 4, Table S6). Thus, typical absorption bands of lipids were indicated in the zone 1 (3000–2800 cm^{-1}); characteristic absorption bands corresponding to protein molecules (and to some sugar) have been framed in the zone 2 (1750–1500 cm^{-1}); typical absorption bands representing the polysaccharides pattern were located in the zone 3 (1100–950 cm^{-1}). The integrated intensities of the absorption zones 1 and 3 were normalized to that of zone 2 (Table S6). Regarding *B. europaea*, the SOM spectra showed a stronger integrated intensity absorption due to the polysaccharidic regions respect *B. regia* and *B. elegans* (Table S6), whereas in *B. regia*, the normalized intensity of the lipids region was the strongest among the species. Then a Mann–Whitney statistical test was carried out to verify if the differences in the relative zone absorption intensities between SOMs of the different species were significant. The statistical analysis didn't show differences in the relative intensity of the three zones between the species. The FTIR spectra of intraskeletal components of SOMs extracted from each species showed weak bands at around 1230/33 cm^{-1} that can be associated with the S═O stretching, suggesting the presence of sulphate groups (acid polysaccharides).

Several attempts were conducted to analyze protein components of the soluble organic matrix extracted from the exoskeletons of the three coral species. The most consistent electrophoresis pattern of SOMs are shown as gel lanes in Fig. 5A-B, alongside with the standard proteins of known molecular weights. The concentration values of proteins in the SOMs separated by SDS-PAGE were: 6.08 mg/ml ± 0.04 for *B. elegans*, 3.26 ± 0.23 mg/ml for *B. regia*, and 1.02 ± 0.02 mg/ml for *B. europaea*. The gel revealed several macromolecular species with molecular masses ranging from ca. 12 to 110 kDa. In *B. elegans,* the SDS-PAGE (Fig. 5A) analysis of the decalcified samples revealed many diffuse bands distributed from ~12 kDa to 50 kDa, with the presence of lower molecular weight molecules (ca. 12 kDa, 15 kDa, 20 kDa, 22 kDa) compared to *B. europaea* and *B. regia.* The SOM fraction of *B. regia* was characterized by the presence of two protein smears (diffused bands) of similar macromolecular species also revealed in *B. europaea*, one around 50 kDa and another from ca. 80–110 kDa (Fig. 5B). In *B. europaea*, macromolecular species, gathered around three main molecular weight distributions, having molecular masses from about 30 to 45 kDa (three discrete weak bands), from about 60 to 75 kDa (three discrete bands most strongly stained) and from ca. 80 to 100 kDa (three discrete weak bands) (Fig. 5B).

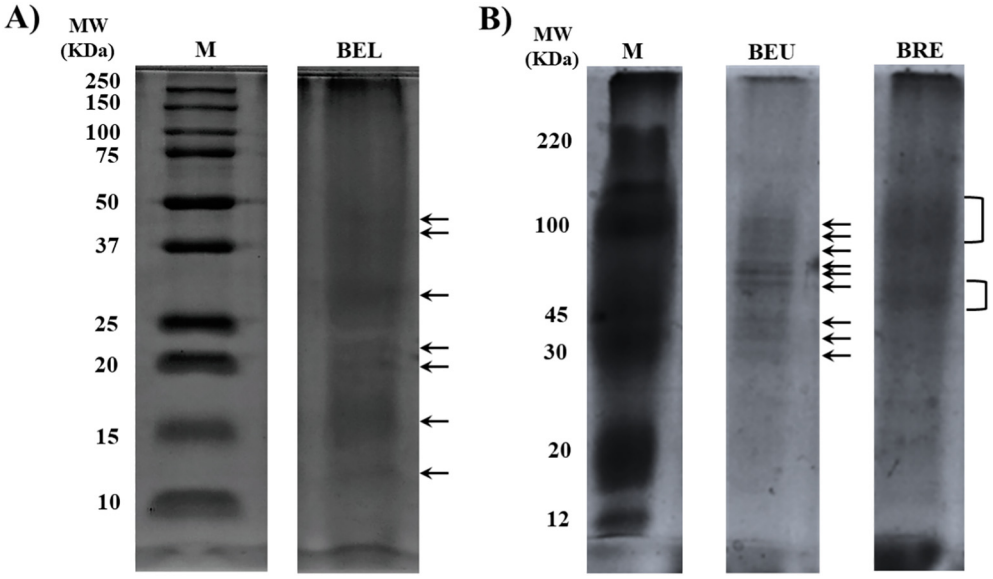

Fig. 5. SDS-PAGE of intra-skeletal SOM extracted from skeletons of *B. elegans* (BEL), *B. regia* (BRE), and *B. europaea* (BEU). The side numbers indicate the molecular weight (MW kDa) of the protein marker (M). A) Protein Marker: BIORAD Precision Plus Protein Dual Color Standard. The protein concentration value was 6.08 ± 0.04 mg/ml for BEL. The volume loaded in the gel lane was 12.3 μl. The arrows indicate the major protein bands. B) Protein Marker: SIGMA ColorBurst Electrophoresis Marker. The protein concentration values, measured by BCA analysis, were 1.02 ± 0.02 mg/ml for BEU and 3.26 ± 0.23 mg/ml for BRE. The volumes applied in the gel lane were 12.0 μl for each species. The arrows indicate the major protein bands and the brackets show the smear band regions.

3.7. OM lipid content and fatty acid analysis

The intra-skeletal FAs concentration (as mass %) were homogeneous among the three species (Kruskal Wallis test, $p > 0.05$; Table 1). *Balanophyllia elegans* showed a skeletal FA content of 0.035 ± 0.013 wt% (mean ± SD), *B. regia* 0.127 ± 0.104 wt%, and *B. europaea* of 0.133 ± 0.122 wt%. Table S7 lists the FA composition (relative distribution %) of the extracts. The detected chain length ranged from C14:0 to C20:0; C16:1, C18:1 and C20:1 were also observed. Missing FA composition data is probably due to values below detection limit (μg). Differences among species were shown in the relative distributions % of C14:0, C15:0, C16:0, C18:0. The FA composition of C14:0 was significantly higher in *B. elegans* (4.5 ± 0.1%) compared to *B. regia* (3.1 ± 0.6%) and *B. europaea* (1.4 ± 0.7%), which showed a lower relative distribution among species (Mann Whitney *U* test $p < 0.05$ Table S7). C15:0 was detected in *B. regia* (2.5 ± 0.4%) and *B. europaea* (0.4 ± 0.1%), but not in *B. elegans*, and showed statistically significant difference between *B. europaea* and the azooxanthellate species (Mann Whitney U test $p < 0.05$ Table S7). C16:0 was the most abundant FA in all the species and showed difference in its relative distribution among species: it was higher in *B. europaea* (51.4 ± 11.3%) compared to *B. regia* (35.4 ± 6.8%) (Mann Whitney U test $p < 0.01$ Table S7), while no statistically significant differences were found in the comparison *B. europaea-B. elegans* and between the azooxanthellate species (Mann Whitney U test $p > 0.05$ Table S7). C18:0 was the second most abundant FA in all the species. Its relative distribution showed differences between *B. elegans* (42.5 ± 5.0%), *B. regia* (25.0 ± 14.3%) and *B. europaea* (21.1 ± 7.0%) with a higher amount in the former compared to the latter (Mann Whitney U test $p < 0.001$ Table S7), a statistically significant difference between the azooxanthellate species (Mann Whitney U test $p < 0.01$ Table S7), and no differences between *B. regia* and *B. europaea* (Mann Whitney U test $p > 0.05$ Table S7). The third most abundant FA detected in all the species was C18:1, ranging from 11.6 ± 5.5% in *B. elegans* to 19.4 ± 8.0% in *B. regia*, but no differences were found among species. C16:1, C17:0, C20:0 and C20:1 were observed in *B. regia* and in *B. europaea*, while they were missing in *B. elegans*.

3.8. OM amino acid composition

The amino acid composition of the protein regions of *B. regia* and *B. elegans* SOM is reported in Table S8, where also the amino acid composition data of *B. europaea,* previously investigated in another study, are shown (Goffredo et al., 2011). The SOMs of *B. regia* and *B. elegans* were characterized by a lower content of acidic residues compared to *B. europaea*. The content of acidic residues in *B. elegans* was 44.0 mol% (Asp 35.7 mol%, and Glu 8.3 mol%), in *B. regia* was 49.1 mol% (Asp 41.7 mol%, and Glu 7.5 mol%) and above 56 mol% in *B. europaea*: Asx (aspartate or asparagine residues) 50.0 mol%, and Glx (glutamate or glutamine residues) about 6 mol%. The content of hydrophobic residues was higher in both azooxanthellate species than *B. europaea*. In fact, Gly, Ala, Val, Ile, Leu, Phe and Pro represented about 38.1 mol% and about 35.4 mol% in *B. elegans* and *B. regia*, respectively; while the SOM of *B. europaea* showed a lower amount of hydrophobic residues (30.0 mol%) (Goffredo et al., 2011). In both SOMs of *B. elegans* and *B. regia*, also arginine and lysine, were present, which were absent in *B. europaea*. In all the species, also serine and threonine were detected and showed differences among SOMs species. In fact, Serine was higher in *B. europaea* and represented the 12.2 mol%, while in *B. elegans* was 6.6 mol% and 7.8 mol% in *B. regia*. The threonine amount was lower in *B. europaea* (1.7 mol%) than in *B. elegans* (4.7 mol%) and *B. regia* (3.5 mol%).

4. Discussion

The heterogeneity of the skeletal architecture and composition of Scleractinian corals is an outcome of many factors related to coral performance, habitat characteristics and evolutionary history (Quattrini et al., 2020). This study provides the first multi-scale analysis of the skeletal features of three related species of the genus *Balanophyllia* and characterized by an earlier heterotrophic feeding mode and a more recent mixotrophic one, aiming to assess possible changes in skeletal phenotype related to the onset of mixotrophy.

At the macroscale (relating to feature sizes >10 μm), an allometric relationship was found between polyp width and length with a progressive ovalization of the oral disc with increasing polyp size in all species,

regardless of their trophic strategy or habitat. A previous study conducted along a Mediterranean latitudinal gradient showed the same trend with increasing polyp age in *B. europaea* (Goffredo et al., 2007). The morphology of the oral discs has been put in relation to sediment disturbances in habitat with high levels of sedimentation (PLA et al., 2012). In fact, the progressive ovalization of the oral disc with increasing length has been considered a strategy to reduce the surface available for sediment accumulation, to increase runoff of sediment and to prevent damage from this stressor, which might occur as polyps become larger (Goffredo et al., 2004; Goffredo et al., 2007; PLA et al., 2012). A different relationship between polyp length and height was found between the zooxanthellate species and the two azooxanthellate counterparts. *B. europaea* showed a positive allometric growth, with polyp height increasing more quickly than polyp length, while both *B. regia* and *B. elegans* presented an isometric growth, with polyp height and length increasing with the same ratio. The allometric behavior shown in *B. europaea* may be another adaptation to sedimentation stress, as this species lives attached to rocky substrata in the shallow waters of the Ligurian Sea, exposed to strong hydrodynamism. Thus, having a higher corallite may help contrast the deposition of sediments on the polyp oral disc.

Here we show that the zooxanthellate *B. europaea* forms larger, denser and less porous skeletons compared to its azooxanthellate sister species. A possible explanation could be that symbiotic corals tend to show higher growth rates compared to non-symbiotic ones (Samorì et al., 2017). In fact, symbiotic algae (zooxanthellae) play an important role in the calcification process of their coral hosts (Iwasaki et al., 2016) through a process known as light enhanced calcification, with calcification being on average three times higher in light than in darkness (Gattuso et al., 1999), thus affecting the size and skeletal density of organisms (Iwasaki et al., 2016).

At the micro-scale the SEM observation (Fig. 2) did not showed a clear pattern in the distribution of the center of calcification in the coral skeleton that can suggest differences among the three species. However, the texture of the fibrous region was quite similar among the three species. This is in line with the model of coral growth reported in the literature that indicated the same mineral building block are used to build up the coral skeleton (Sun et al., 2020).

At the nano-scale, (relating to feature sizes <1 μm) the mean value of micro-density of *B. regia* was significantly lower compared to the other two species as a result of a higher content of extra-mineral phases (e.g. calcite, magnesium-calcite) having lower density (2.94 g cm^{-3} for aragonite, 2.71 g cm^{-3} for calcite, (Marszalek, 1982)) in the coral skeletons. The higher percentage of extra-mineral calcium carbonate polymorphs founded in *B. regia* may be due to the presence of boring organisms (e.g., sponges, polychaetes, bivalves, cyanobacteria, microalgae and fungi), which produce calcite and magnesium-calcite (Brahmi et al., 2010), thus adding exogenous mineral phases in the coral skeleton, while digging galleries (small holes) inside the coral skeletons (Goffredo et al., 2012). Furthermore, the more porous and potentially fragile skeletal phenotype of *B. regia* and its shallow depth compared to *B. elegans* could favour the establishment of boring organisms within its skeleton (Maher et al., 2018). Calcite and magnesium-calcite were found in addition to aragonite in all species, in agreement with previous studies conducted on scleractinian corals (Goffredo et al., 2012; Stolarski et al., 2021). In *B. regia* and *B. elegans* quartz was also detected. The puzzling presence of these additional mineral phases in the skeleton can be hypothesized due to diverse causes. Indeed, previous studies suggest that the distribution of the different $CaCO_3$ forms inside skeletons of scleractinian corals may result from different mechanisms: 1) Corals may biologically precipitate calcite crystals at their early stages in order to ensure their settlement on the substrate of fixation; (2) Mg-calcite presence may come out from skeletons of other calcifying organisms such as crustose coralline algae; in fact, crustose coralline algae are almost exclusively (98–100%) made of high Mg-calcite; and/or (3) calcite may be interpreted as diagenetic infilling of microborer cavities, which are known to colonize coral skeletons (Goffredo et al., 2012; Stolarski et al., 2021). The presence of quartz may be due to boring organism such as sponges composed of silica spicules which may enter in the skeleton of corals (Rützler, 2012), or/and due to sediment particles (containing quartz) that may be trapped in the growing skeleton. It is likely that more than one of the above mentioned processes contribute to explaining the higher content of external mineral phases in the skeletons of *B. regia* and *B. elegans* compared to *B. europaea*. However, crystallite size and microstrain fluctuation resulted homogeneous among species, suggesting that the basic building blocks of aragonite crystals remained a conserved trait in these three related species. Thermograms showed a first weight loss in a range around 125–250 °C (related to the loss of structured water) followed by one between about 250 °C and 450 °C (generally associated with organic matrix pyrolysis) (Reggi et al., 2014). The results of the thermogravimetric OM investigations of the corals *B. europaea*, *B. regia* and *B. elegans* showed a possible relationship between trophic strategy and the intra-skeletal OM content. In fact, a higher OM content was reported in *B. europaea* (*w*/*w* 2.30 ± 0.44%) compared to *B. regia* (*w*/*w* 2.04 ± 0.37%) and *B. elegans* (*w*/*w* 1.99 ± 0.27%). This could be the result of the additional phototrophic supplies provided by the symbiotic dinoflagellates to the coral host in terms of macromolecules and energy (Muscatine et al., 1989). The higher content in intra-skeletal OM, which contains proteins, polysaccharides and lipids that promote the precipitation of $CaCO_3$ (Falini et al., 2015), could also explain the higher growth rates and therefore higher bulk density reported in this study for the zooxanthellate species. The intra-skeletal organic matrix (OM) content was not related to polyp length and skeletal mass in either species, suggesting that the ontogenesis of the investigated species does not affect the OM.

The quantitative differences between the zooxanthellate and the two azooxanthellate species highlighted by the coral skeletal features agree with the PCA analysis (Fig. S9) which shows two main clusters, one for *B. elegans* and *B. regia* and one for *B. europaea* (Fig. S9).

The SDS-PAGE observations of the SOM revealed several proteins with molecular masses ranging from ca. 30 to 100 kDa in *B. europaea*, from about 50 kDa to 110 kDa in *B. regia* and from ca. 12 to 50 kDa in *B. elegans*. The discrete bands identified in *B. europaea* matched with previously observations (Goffredo et al., 2011), showing bands clustered in three groups having molecular masses from about 30 to 45 kDa, from ca. 60 to 75 kDa and around 80–100 kDa. On the other hand, the SOMs of *B. regia* and *B. elegans* resulted in a smear of polydisperse macromolecules (diffuse color). A possible explanation for the smeary pattern in the azooxanthellate species could be due to post-translational modifications which may lead to polydisperse macromolecules and glycosylated proteins in their SOMs that mask the identification of discrete protein bands and create blurry and thick bands (Marin et al., 2016). Indeed, the amino acid composition revealed only in the azooxanthellate species the presence of arginine and lysine, which can interact with negatively charged ions (bicarbonate) or acidic matrix proteins (Mass et al., 2016). In particular, the lysine residues act as glycosylation sites and arginine as phosphorylatation ones and allow for protein post-translational modifications (Alvares, 2014). Therefore, the presence of these residues suggests the presence of glycosylated/phosphorylated proteins in the SOMs of *B. regia* and *B. elegans* that may have the capacity to bind calcium ions creating the observed smeary pattern (Mass et al., 2013). Previous studies have highlighted differences in biochemical composition of organic matrices of symbiotic and non-symbiotic corals, suggesting an involvement of zooxanthellae in the organic matrix composition, probably indirectly, through the synthesis of precursors which are assembled by calicoblastic cells to form organic matrix which is then secreted (Puverel et al., 2005). Nevertheless, also the food source might act directly by providing external amino acids necessary for organic matrix or by supplying additional energy for protein synthesis (Houlbreque, 2004). The

intra-skeletal fatty acids concentration (as mass %) were homogeneous among the species and, differently as previously reported data (Samorì et al., 2017), we didn't find any trend of higher FA concentration in zooxanthellate than in azooxanthellate corals, probably due to different environmental conditions which may influence the FA contents and compositions (Radice et al., 2019). Whereas, the OM fatty acid composition revealed differences likely linked to the different energy intake strategies. The analysis obtained by gas chromatography–mass spectrometry (GC–MS) revealed that, for all the species, palmitic acid (C16:0) was the most abundant fatty acid, followed by stearic (C18:0) and oleic acid (C18:1) in order of concentration. The first two fatty acids indicate omnivorous or carnivorous feeding modes (Sargent and McIntosh, 1974), whereas the last fatty acid (C18:1) was previously found only in the skeleton of symbiotic coral (Samorì et al., 2017) since it is likely a photosynthesis-derived product (Matthews et al., 2018). The fact that we detected oleic acid in the skeleton of azooxanthellate corals, that exclusively rely on heterotrophic feeding, indicates that phytoplankton is the most probable source of this fatty acid, assumed directly by the coral or indirectly by feeding on zooplankton whose diet is based on phytoplankton (Fox et al., 2018).

5. Conclusions

In conclusion, the comparative analysis reported in this study suggests that the onset of mixotrophy might have left a fingerprint on the skeletal structural features of these three related species of the genus *Balanophyllia*. However, further studies under controlled conditions of lighting and nutrient supply in aquaria are needed to confirm this conclusion. The current study adds to the growing body of literature highlighting the remarkable plasticity of coral skeletons which repeatedly allowed this coral group to adapt to a range of changing environments throughout its geological history.

CRediT authorship contribution statement

Quinzia Palazzo: Investigation, Formal analysis, Writing – original draft, Visualization. **Fiorella Prada:** Investigation, Formal analysis, Writing – original draft. **Tim Steffens:** Investigation. **Simona Fermani:** Investigation. **Chiara Samorì:** Investigation. **Giacomo Bernardi:** Resources, Writing – review & editing. **Alexis Terrón-Sigler:** Resources, Writing – review & editing. **Francesca Sparla:** Investigation, Resources, Writing – review & editing, Supervision. **Giuseppe Falini:** Conceptualization, Resources, Writing – review & editing, Supervision, Project administration. **Stefano Goffredo:** Conceptualization, Resources, Writing – review & editing, Supervision, Project administration.

Declaration of competing interest

The authors declare that they have no known competing financial interests or personal relationships that could have appeared to influence the work reported in this paper.

Acknowledgments

The research leading to these results has received funding from the European Research Council under the European Union's Seventh Framework Program (FP7/2007-2013)/ERC grant agreement no. 249930 (CoralWarm: Corals and global warming: the Mediterranean versus the Red Sea). The diving center Bubble Lounge Diving provided logistic assistance in the underwater activities at Genova. The research leading to these results has been conceived under the International PhD Program "Innovative Technologies and Sustainable Use of Mediterranean Sea Fishery and Biological Resources" (www.FishMed-PhD.org). This study represents partial fulfilment of the requirements for the Ph.D. thesis of Quinzia Palazzo.

Supplementary data

Supplementary data to this article can be found online at https://doi.org/10.1016/j.scitotenv.2021.148778.

References

Alvares, K., 2014. The role of acidic phosphoproteins in biomineralization. Connect. Tissue Res. 55, 34–40. https://doi.org/10.3109/03008207.2013.867336.
Arrigoni, R., Kitano, Y.F., Stolarski, J., Hoeksema, B.W., Fukami, H., Stefani, F., et al., 2014. A phylogeny reconstruction of the Dendrophylliidae (Cnidaria, Scleractinia) based on molecular and micromorphological criteria, and its ecological implications. Zool. Scr. 43, 661–688. https://doi.org/10.1111/zsc.12072.
Bosellini, F.R., Perrin, C., 2008. Estimating Mediterranean Oligocene–Miocene sea-surface temperatures: an approach based on coral taxonomic richness. Palaeogeogr. Palaeoclimatol. Palaeoecol. 258, 71–88. https://doi.org/10.1016/j.palaeo.2007.10.028.
Brahmi, C., Meibom, A., Smith, D.C., Stolarski, J., Auzoux-Bordenave, S., Nouet, J., et al., 2010. Skeletal growth, ultrastructure and composition of the azooxanthellate scleractinian coral Balanophyllia regia. Coral Reefs 29, 175–189. https://doi.org/10.1007/s00338-009-0557-x.
Cairns, S.D., 2001. A generic revision and phylogenetic analysis of the Dendrophylliidae (Cnidaria: Scleractinia). Smithson Contrib to Zool, pp. 1–75 https://doi.org/10.5479/si.00810282.615.
Campoy, A.N., Addamo, A.M., Machordom, A., Meade, A., Rivadeneira, M.M., Hernández, C.E., et al., 2020. The origin and correlated evolution of symbiosis and coloniality in scleractinian corals. Front. Mar. Sci. 7. https://doi.org/10.3389/fmars.2020.00461.
Caroselli, E., Prada, F., Pasquini, L., Marzano, F.N., Zaccanti, F., Falini, G., et al., 2011. Environmental implications of skeletal micro-density and porosity variation in two scleractinian corals. Zoology 114, 255–264. https://doi.org/10.1016/j.zool.2011.04.003.
Caroselli, E., Nanni, V., Levy, O., Falini, G., Dubinsky, Z., Goffredo, S., 2015. Latitudinal variations in biometry and population density of a Mediterranean solitary coral. Limnol. Oceanogr. 60, 1356–1370. https://doi.org/10.1002/lno.10100.
Coates, A.G., Obando, J.A., 1996. The geologic evolution of the Central American Isthmus. Evol. Environ. Trop. Am. 21–56.
Cuif, J.-P., Dauphin, Y., Berthet, P., Jegoudez, J., 2004. Associated water and organic compounds in coral skeletons: quantitative thermogravimetry coupled to infrared absorption spectrometry. Geochem. Geophys. Geosyst. 5. https://doi.org/10.1029/2004GC000783 n/a-n/a.
Dishon, G., Grossowicz, M., Krom, M., Guy, G., Gruber, D.F., Tchernov, D., 2020. Evolutionary traits that enable scleractinian corals to survive mass extinction events. Sci. Rep. 10, 3903. https://doi.org/10.1038/s41598-020-60605-2.
Fadlallah, Y.H., 1983a. Population dynamics and life history of a solitary coral, Balanophyllia elegans, from Central California. Oecologia 58, 200–207. https://doi.org/10.1007/BF00399217.
Fadlallah, Y.H., 1983b. Sexual reproduction, development and larval biology in scleractinian corals. Coral Reefs 2, 129–150. https://doi.org/10.1007/BF00336720.
Fadlallah, Y.H., Pearse, J.S., 1982. Sexual reproduction in solitary corals: overlapping oogenic and brooding cycles, and benthic planulas in Balanophyllia elegans. Mar. Biol. 71, 223–231. https://doi.org/10.1007/BF00397039.
Falini, G., Fermani, S., Goffredo, S., 2015. Coral biomineralization: a focus on intra-skeletal organic matrix and calcification. Semin. Cell Dev. Biol. 46, 17–26. https://doi.org/10.1016/j.semcdb.2015.09.005.
Foster, M.S., Reed, D.C., Carr, M.H., Dayton, P.K., Malone, D.P., Pearse, J.S., et al., 2013. Kelp forests in California. In research and discoveries: the revolution of science through scuba. Smithson. Contrib. Mar. Sci. 115–132.
Fox, M.D., Williams, G.J., Johnson, M.D., Radice, V.Z., Zgliczynski, B.J., Kelly, E.L.A., et al., 2018. Gradients in primary production predict trophic strategies of mixotrophic corals across spatial scales. Curr. Biol. 28, 3355–3363.e4. https://doi.org/10.1016/j.cub.2018.08.057.
Gattuso, J.-P., Allemand, D., Frankignoulle, M., 1999. Photosynthesis and calcification at cellular, organismal and community levels in coral reefs: a review on interactions and control by carbonate chemistry. Am. Zool. 39, 160–183. https://doi.org/10.1093/icb/39.1.160.
Gerrodette, T., 1981. Dispersal of the solitary coral balanophyllia elegans by demersal planular larvae. Ecology 62, 611–619. https://doi.org/10.2307/1937728.
Goffredo, S., Telò, T., Scanabissi, F., 2000. Ultrastructural observations of the spermatogenesis of the hermaphroditic solitary coral Balanophyllia europaea (Anthozoa, Scleractinia). Zoomorphology https://doi.org/10.1007/PL00008495.
Goffredo, S., Mattioli, G., Zaccanti, F., 2004. Growth and population dynamics model of the Mediterranean solitary coral Balanophyllia europaea (Scleractinia, Dendrophylliidae). Coral Reefs 23, 433–443. https://doi.org/10.1007/s00338-004-0395-9.
Goffredo, S., Caroselli, E., Pignotti, E., Mattioli, G., Zaccanti, F., 2007. Variation in biometry and population density of solitary corals with solar radiation and sea surface temperature in the Mediterranean Sea. Mar. Biol. 152, 351–361. https://doi.org/10.1007/s00227-007-0695-z.
Goffredo, S., Caroselli, E., Mattioli, G., Pignotti, E., Zaccanti, F., 2008. Relationships between growth, population structure and sea surface temperature in the temperate solitary coral Balanophyllia europaea (Scleractinia, Dendrophylliidae). Coral Reefs 27, 623–632. https://doi.org/10.1007/s00338-008-0362-y.
Goffredo, S., Caroselli, E., Mattioli, G., Pignotti, E., Dubinsky, Z., Zaccantia, F., 2009. Inferred level of calcification decreases along an increasing temperature gradient in a Mediterranean endemic coral. Limnol. Oceanogr. 54, 930–937. https://doi.org/10.4319/lo.2009.54.3.0930.

Goffredo, S., Vergni, P., Reggi, M., Caroselli, E., Sparla, F., Levy, O., et al., 2011. The skeletal organic matrix from Mediterranean coral balanophyllia europaea influences calcium carbonate precipitation. PLoS One 6, e22338. https://doi.org/10.1371/journal.pone.0022338.

Goffredo, S., Caroselli, E., Mezzo, F., Laiolo, L., Vergni, P., Pasquini, L., et al., 2012. The puzzling presence of calcite in skeletons of modern solitary corals from the Mediterranean Sea. Geochim. Cosmochim. Acta 85, 187–199. https://doi.org/10.1016/j.gca.2012.02.014.

Houlbreque, F., 2004. Interactions between zooplankton feeding, photosynthesis and skeletal growth in the scleractinian coral Stylophora pistillata. J. Exp. Biol. 207, 1461–1469. https://doi.org/10.1242/jeb.00911.

Iwasaki, S., Inoue, M., Suzuki, A., Sasaki, O., Kano, H., Iguchi, A., et al., 2016. The role of symbiotic algae in the formation of the coral polyp skeleton: 3-D morphological study based on X-ray microcomputed tomography. Geochem. Geophys. Geosyst. 17, 3629–3637. https://doi.org/10.1002/2016GC006536.

Kerr, A.M., Baird, A.H., Hughes, T.P., 2011. Correlated evolution of sex and reproductive mode in corals (Anthozoa: Scleractinia). Proc. R. Soc. B Biol. Sci. 278, 75–81. https://doi.org/10.1098/rspb.2010.1196.

Langford, J.I., Wilson, A.J.C., 1978. Scherrer after sixty years: a survey and some new results in the determination of crystallite size. J. Appl. Crystallogr. 11, 102–113. https://doi.org/10.1107/S0021889878012844.

Lyle, M., Barron, J., Bralower, T.J., Huber, M., Olivarez Lyle, A., Ravelo, A.C., et al., 2008. Pacific Ocean and Cenozoic evolution of climate. Rev. Geophys. 46, RG2002. https://doi.org/10.1029/2005RG000190.

Maher, R.L., Johnston, M.A., Brandt, M.E., Smith, T.B., Correa, A.M.S., 2018. Depth and coral cover drive the distribution of a coral macroborer across two reef systems. PLoS One 13, e0199462. https://doi.org/10.1371/journal.pone.0199462.

Marchegiani, F., Cibej, E., Vergni, P., Tosi, G., Fermani, S., Falini, G., 2009. Hydroxyapatite synthesis from biogenic calcite single crystals into phosphate solutions at ambient conditions. J. Cryst. Growth 311, 4219–4225. https://doi.org/10.1016/j.jcrysgro.2009.07.010.

Marin, F., Immel, F., Trinkler, N., Gaspard, D., 2016. Staining SDS-PAGE gels of skeletal matrices after western blot: a way to improve their sharpness. Key Eng. Mater. 672, 215–221. https://doi.org/10.4028/www.scientific.net/KEM.672.215.

Marszalek, D.S., 1982. The role of heavy skeletons in vertical movements of nonmotile zooplankton. Mar. Behav. Physiol. 8, 295–303. https://doi.org/10.1080/10236248209387026.

Martín, J.M., Braga, J.C., Sánchez-Almazo, I.M., Aguirre, J., 2012. Temperate and Tropical Carbonatesedimentation Episodes in the Neogene Betic Basins (Southern Spain) Linked to cLimatic Oscillations and Changes in Atlantic-Mediterranean Connections: Constraints from Isotopic Data. Carbonate Syst. Dur. Oligocene-Miocene Clim. Transit. Wiley-Blackwell, Oxford, UK, pp. 49–69 https://doi.org/10.1002/9781118398364.ch4.

Mass, T., Drake, J.L., Haramaty, L., Kim, J.D., Zelzion, E., Bhattacharya, D., et al., 2013. Cloning and characterization of four novel coral acid-rich proteins that precipitate carbonates in vitro. Curr. Biol. 23, 1126–1131. https://doi.org/10.1016/j.cub.2013.05.007.

Mass, T., Putnam, H.M., Drake, J.L., Zelzion, E., Gates, R.D., Bhattacharya, D., et al., 2016. Temporal and spatial expression patterns of biomineralization proteins during early development in the stony coral Pocillopora damicornis. Proc. R. Soc. B Biol. Sci. 283, 20160322. https://doi.org/10.1098/rspb.2016.0322.

Matthews, J.L., Oakley, C.A., Lutz, A., Hillyer, K.E., Roessner, U., Grossman, A.R., et al., 2018. Partner switching and metabolic flux in a model cnidarian–dinoflagellate symbiosis. Proc. R. Soc. B Biol. Sci. 285, 20182336. https://doi.org/10.1098/rspb.2018.2336.

Misic, C., Castellano, M., Covazzi Harriague, A., 2011. Organic matter features, degradation and remineralisation at two coastal sites in the Ligurian Sea (NW Mediterranean) differently influenced by anthropogenic forcing. Mar. Environ. Res. 72, 67–74. https://doi.org/10.1016/j.marenvres.2011.05.006.

Muscatine, L., Falkowski, P.G., Dubinsky, Z., Cook, P.A., McCloskey, L.R., 1989. The effect of external nutrient resources on the population dynamics of zooxanthellae in a reef coral. Proc. R. Soc. Lond. B Biol. Sci. 236, 311–324. https://doi.org/10.1098/rspb.1989.0025.

Pandolfi, J.M., Jackson, J.B.C., 2001. Community structure of Pleistocene coral reefs of Curaçao, Netherlands Antilles. Ecol. Monogr. 71, 49–67. https://doi.org/10.1890/0012-9615(2001)071[0049:CSOPCR]2.0.CO;2.

PLA, Erftemeijer, Riegl, B., Hoeksema, B.W., Todd, P.A., 2012. Environmental impacts of dredging and other sediment disturbances on corals: a review. Mar. Pollut. Bull. 64, 1737–1765. https://doi.org/10.1016/j.marpolbul.2012.05.008.

Puverel, S., Tambutté, E., Zoccola, D., Domart-Coulon, I., Bouchot, A., Lotto, S., et al., 2005. Antibodies against the organic matrix in scleractinians: a new tool to study coral biomineralization. Coral Reefs 24, 149–156. https://doi.org/10.1007/s00338-004-0456-0.

Quattrini, A.M., Rodríguez, E., Faircloth, B.C., Cowman, P.F., Brugler, M.R., Farfan, G.A., et al., 2020. Palaeoclimate ocean conditions shaped the evolution of corals and their skeletons through deep time. Nat. Ecol. Evol. https://doi.org/10.1038/s41559-020-01291-1.

Radice, V.Z., Brett, M.T., Fry, B., Fox, M.D., Hoegh-Guldberg, O., Dove, S.G., 2019. Evaluating coral trophic strategies using fatty acid composition and indices. PLoS One 14, e0222327. https://doi.org/10.1371/journal.pone.0222327.

Reggi, M., Fermani, S., Landi, V., Sparla, F., Caroselli, E., Gizzi, F., et al., 2014. Biomineralization in Mediterranean corals: the role of the intraskeletal organic matrix. Cryst. Growth Des. 14, 4310–4320. https://doi.org/10.1021/cg5003572.

Rützler, K., 2012. The role of sponges in the Mesoamerican barrier-reef ecosystem, Belize. Adv. Mar. Biol., 211–271 https://doi.org/10.1016/B978-0-12-387787-1.00002-7.

Samorì, C., Caroselli, E., Prada, F., Reggi, M., Fermani, S., Dubinsky, Z., et al., 2017. Ecological relevance of skeletal fatty acid concentration and composition in Mediterranean scleractinian corals. Sci. Rep. 7, 1929. https://doi.org/10.1038/s41598-017-02034-2.

Sargent, J.R., McIntosh, R., 1974. Studies on the mechanism of biosynthesis of wax esters in Euchaeta norvegica. Mar. Biol. 25, 271–277. https://doi.org/10.1007/BF00404969.

Stanley, G.D., 2003. The evolution of modern corals and their early history. Earth Sci. Rev. 60, 195–225. https://doi.org/10.1016/S0012-8252(02)00104-6.

Stanley, G.D., van de Schootbrugge, B., 2009. The Evolution of the Coral–Algal Symbiosis. , pp. 7–19 https://doi.org/10.1007/978-3-540-69775-6_2.

Stolarski, J., Coronado, I., Murphy, J.G., Kitahara, M.V., Janiszewska, K., Mazur, M., et al., 2021. A modern scleractinian coral with a two-component calcite–aragonite skeleton. Proc. Natl. Acad. Sci. 118, e2013316117. https://doi.org/10.1073/pnas.2013316117.

Sun, C.-Y., Stifler, C.A., Chopdekar, R.V., Schmidt, C.A., Parida, G., Schoeppler, V., et al., 2020. From particle attachment to space-filling coral skeletons. Proc. Natl. Acad. Sci. 117, 30159–30170. https://doi.org/10.1073/pnas.2012025117.

Tambutté, S., Holcomb, M., Ferrier-Pagès, C., Reynaud, S., Tambutté, É., Zoccola, D., et al., 2011. Coral biomineralization: from the gene to the environment. J. Exp. Mar. Biol. Ecol. 408, 58–78. https://doi.org/10.1016/j.jembe.2011.07.026.

Terrón-Sigler, A., López-González, P.J., 2005. Cnidae variability in Balanophyllia europaea and B. regia (Scleractinia: Dendrophylliidae) in the NE Atlantic and Mediterranean Sea. Sci. Mar. 69, 75–86.

Terrón-Sigler, A., León-Muez, D., Peñalver-Duque, P., Gálvez-César, R., Espinosa Torre, F., 2016. Geographic distribution of Astroides calycularis (Scleractinia: Dendrophylliidae) as a baseline to assess future human impacts on the southern Iberian Peninsula. J. Mar. Biol. Assoc. UK https://doi.org/10.1017/S0025315415001113.

Toby, B.H., 2005. CMPR – a powder diffraction toolkit. J. Appl. Crystallogr. 38, 1040–1041. https://doi.org/10.1107/S0021889805030232.

Todd, P.A., 2008. Morphological plasticity in scleractinian corals. Biol. Rev. 83, 315–337. https://doi.org/10.1111/j.1469-185X.2008.00045.x.

Vaughan, T.W., Wells, J.W., 1943. Revision of the suborders families, and genera of the Scleractinia. Spec. Pap. Geol. Soc. Am., 1–394 https://doi.org/10.1130/SPE44-p1.

Vertino, A., Stolarski, J., Bosellini, F.R., Taviani, M., 2014. Mediterranean Corals Through Time: From Miocene to Present. Mediterr. Sea. Springer Netherlands, Dordrecht, pp. 257–274 https://doi.org/10.1007/978-94-007-6704-1_14.

Zibrowius, H., 1980. Les Scleractiniaires de la Mediterranee et de l'Atlantique nord-oriental. Mem l'Institut Oceanogr Monaco 11, 284.

Zolotoyabko, E., 2014. Basic Concepts of X-ray Diffraction.